Hindawi
International Journal of Photoenergy
Volume 2021, Article ID 1214170, 10 pages
https://doi.org/10.1155/2021/1214170

Research Article

Fabrication of p-NiO/n-TiO_2 Solar Device for Photovoltaic Application

R. T. Mouchou,[1] **K. O. Ukoba**,[1] **O. T. Laseinde**,[2] **and T. C. Jen**[1]

[1]*University of Johannesburg, Auckland Park Campus, Johannesburg, South Africa*
[2]*University of Johannesburg, Doornfontein Campus, Johannesburg, South Africa*

Correspondence should be addressed to T. C. Jen; tjen@uj.ac.za

Received 30 July 2021; Revised 22 September 2021; Accepted 18 October 2021; Published 26 November 2021

Academic Editor: Joaquim Carneiro

Energy demand is increasing globally owing to population growth. Solar cell development has gained considerable attention because of its potential to provide everyone with sustainable, affordable, clean, and globally accessible energy. A heterojunction solar device for photovoltaic applications was developed in this study, using nickel oxide (NiO) as the p-type and titanium oxide (TiO2) as the n-type. The material chosen was motivated by the affordability, availability, and performance compared to existing silicon that is more efficient but less affordable and available. The TiO_2 and NiO_2 were synthesised and characterised before the deposition and characterisation of the solar cells. The characterisation was carried out using Fourier transform infrared spectroscopy (FTIR), Transmission Electron Microscopy (TEM), scanning electron microscopy (SEM), EDX, X-ray Diffraction (XRD), and a four-point probe. The deposition parameters were fine-tuned to achieve optimum optoelectronic properties for the solar device. The final device exhibited an open-circuit voltage of 370 mV, a current density of 1.7 mA, and solar cells efficiency of 3.7.

1. Introduction

The world is undergoing a new era of industrialisation characterised by sustainable energy sources, fast internet, and disruptive technologies. This era is popularly referred to as Industry 4.0. Despite the revolutionary changes in sustainable energy generation, many developing countries struggle with a lack of electric power supply. A clean, sustainable, and affordable energy access is critical for countries to benefit from the industrial revolution. Solar energy is among the energy options with the promise of being clean, sustainable, and affordable [1]. This study is aimed at improving solar cells' by fabricating a heterojunction p-NiO/n-TiO_2 using spin coating, spray pyrolysis, and DC Magnetron sputtering. Improving the open-circuit voltage, short-circuit current density, and fill factor will improve efficiency [2]. Solar cells have experienced a transition with emphasis on cost, toxicity, and efficiency. The first generation of solar cells was an inorganic silicon wafer that had high efficiency but high cost. The second generation is inorganic thin films (CIGS, CdTe) with high efficiency but toxic and harmful to the environment. The third-generation solar cells are organic thin films with ease of processing AND low cost but improved efficiency. Different deposition techniques have been used for the deposition of heterojunction solar cells [3–8]. These deposition techniques are classified using various parameters of cost, simplicity among others [9]. Spin coating and spray pyrolysis are among the low-cost deposition techniques because they are simple and require low maintenance [10–12]. These two methods offer ease of film deposited, control of the coated area, and low equipment cost vital for cost reduction of the deposited film [13, 14].

Metal oxides are being studied as a cost-effective replacement to expensive solar cells materials. They are easy to fine-tune, deposit, and readily available. Researchers are interested in NiO because it is affordable, available, and

stable. This has made researchers tune the conductivity and energy level of NiO to allow usage in solar cell fabrication, including usage for hole transport and window layer. Although the bandgap of NiO is high compared to silicon and ZnO, there has been the usage of NiO for hole transport and as a window layer [15–17]. The bandgap of about 3.5 eV to 4.0 eV and suitability of NiO as a p-type solar cells material has endeared it [18]. NiO has good structural and optical properties [19], good photoabsorption [20], and unique electrical properties [21]. TiO_2 has been used as n-type material with several p-type materials owing to the excellent solar harvesting ability. TiO_2 is highly resistant to photo corrosion, stable in different pH, nontoxic, and affordable [22]. Heterojunction solar cells promise to be stable, cost-effective, and with better efficiency [23]. Tuning of inorganic p-type semiconductors has contributed to improved efficiency [24]. NiO p-type helped in obtaining improved solar efficiency [25]. Ukoba et al. [15] obtained an efficiency of 2.30 using the spray pyrolysis method.

According to the studied literature, the efficiency of NiO/TiO_2 requires improvement despite its potential. This study leverage the potential of spin coating, heterojunction solar cells to improve the solar efficiency compared to existing values. The decision to use spray pyrolysis and spin coating are inexpensive solution-based chemistry methods for fabricating affordable, clean solar cells, especially metal oxide [9]. These methods were used because of the simplicity and low cost of the deposition method. Spray pyrolysis was earlier used for depositing both layers [15]. However, this study decided to use a spin coating to deposit the NiO as it was used for obtaining improved efficiency in the highest efficiency obtained for perovskite by Oxford.

The article is structured such that the introduction is followed by a detailed explanation of how the solar device's substrate is cleaned and precursors are deposited. After that, followed by a review of the characterisation data, a detailed discussion of the results was also done. The article discusses the process of fabricating a solar cell device that generated an efficiency of 3.7 by spin coating, spray pyrolysis, and DC magnetron sputtering. A conclusion is included to demonstrate the study's significant contribution to the existing body of knowledge.

2. Methodology

2.1. Substrate Cleaning. The substrates used are glass and ITO-coated glass. The process used for cleaning the substrates are indicated as follows: substrate wipe, substrate chemically washed, and substrate ultrasonically cleaned. The substrate was wiped to rid the surface of residues and impurities. After that, the substrate was washed in distilled water, methanol, propanol, acetone, and nitrogen to blow dry it. It was also ultrasonically cleaned for complete residue removal before deposition using spin coating technique model CHEMAT TECHNOLOGY spin-coater KW-4A (shown in Figure 1) was used with a time of 30 s, speed of 1,000 rpm.

Figure 1: The model CHEMAT TECHNOLOGY spin-coater used for the fabrication p-NiO/n-TiO_2.

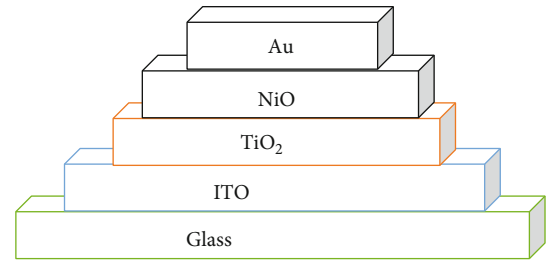

Figure 2: Schematic diagram of the p-NiO/n-TiO_2 solar device.

2.2. Synthesis and Deposition. This study fabricated a solar cells device using spin coating, spray pyrolysis, and magnetron sputtering utilising the structure shown in Figure 2.

Analytical grade chemicals shown in Table 1 were obtained and used for the entirety of the synthesis and deposition.

2.3. Precursor Preparation TiO_2. The TiO_2 precursor was obtained using titanium (IV) isopropoxide 97.0% dissolved in 99.9% ethanol in a 1 : 5 volume ratio while stirring. After stirring for 30 minutes, acid stock prepared by mixing nitric acid with water in the ratio 1 : 50 volume was added into the solution dropwise whilst stirring at 500 rpm minute using a magnetic stirrer. After that, the mixture was further stirred under heating at 100.0°C and dried in Ecotherm Labotec oven at 250.0°C for 24 hrs to obtain the TiO_2 nanoparticles as shown in equation (1).

$$\mathrm{Ti(OC_4H_9)_4 + 2H_2O \longrightarrow TiO_2 + 4C_4H_9OH} \quad (1)$$

2.4. Precursor Preparatio NiO. The precursor solution for NiO was nickel acetate tetrahydrate. The method of [26] was employed with slight modification. To prepare NiO nanoparticles, 5.96 g of nickel acetate monohydrate precursor was dissolved in 50 mL of 2-methoxy ethanol to obtain a 0.2 M solution. Equimolar (0.2 M) ethanolamine (600 mL) was immediately added, and a green coloured homogeneous solution was obtained by vigorous stirring. Once the precursor was dissolved completely, 2 M of NaOH

Table 1: Analytical grade chemicals used for NiO/TiO_2 solar cells.

Materials	Source	Purpose
Titanium (IV) isopropoxide 97.0%	Sigma-Aldrich Germany	As the precursor for TiO_2 synthesis
Nickel acetate	Sigma-Aldrich Germany	As the precursor for NiO synthesis
Ethanol 99.9%	Merck chemicals South Africa	As the solvent for TiO_2 sol-gel
Nitric acid 70.0% reagent	Sigma-Aldrich USA	As stabiliser to avoid precipitation
Deionised water	Merck chemicals South Africa	As sol-hydrolysing agent

was added dropwise to the precursor solution. After the addition of NaOH, the colour of the solution turned dark green. Thereafter, 2 to 3 h of stirring at 60°C after, the solution turned its colour to light brown. The substrate was heated at a constant temperature of 100°C on a heater, as shown in equation (2). Nickel oxide is the final product, as presented in equation (2)

$$Ni(CH_3COO)_2.4H_2O \xrightarrow{heat} NiO + 7H_2O\uparrow + 4CO_2\uparrow \quad (2)$$

These are characterised and discussed in detail before final solar device fabrication to optimise the various layers.

2.5. Characterisation. Standard characterisations were performed to establish the properties of NiO, TiO_2, and the solar device. Molecular bonding and absorption bands of the nanoparticles were characterised using Perkin Elmer Spectrum 100 FT-IR spectrometer in the spectrum range of 4000 cm^{-1} to 300 cm^{-1}. The image and morphology were analysed under a JEOL JEM 2100 80T X-MAX (Oxford) transmission electron microscope (TEM) instrument. MLA software was used to scan electron microscopy on an FEI XL40 ESEM equipped with two EDAX Sapphire Si(Li) EDS detectors.

A Philips XPERT-PRO X-ray diffractometer was used to evaluate the structural composition.

For JV characterisation, a Keithley Source Meter 2400 with a two-point probe was used. The illumination source was a Newport solar simulator with an intensity of (100.0 mW/cm^2), which is explained in detail.

3. Results and Discussion

3.1. Fourier Transform Infrared (FTIR) Analysis. The Fourier transform infrared spectroscopy (FTIR), shown in Figure 3(a), was used to investigate the successful synthesis of nickel oxide nanoparticles. The FTIR bands from 400.0 to 1000.0 cm^{-1} indicates the vibrations of NiO nanoparticles. The Ni-O stretching vibration confirmed the nickel oxide nanoparticles at 483.0 cm^{-1} and Ni-OH at 610.0 cm^{-1}. This obtained Ni-O is within the standard range for NiO [27, 28].

The O-H and C-H stretch was confirmed at 3658.0 and 2882.0 cm^{-1}, respectively. This obtained stretching vibration of NiO is within the band region [29]. The C-O absorption bands were seen at 1106.0 cm^{-1}.

The strong absorption in the region of 400.0 to 1000.0 cm^{-1} represents the Ti-O-Ti modes, as shown in Figure 3(b). The Ti-O stretching vibration was seen at 487.0 cm^{-1}, and the higher Ti-O modes were seen at 1363.0 cm^{-1} which is within the value obtained by Mugundan, Rajamannan [30]. Peaks at 3410.0 and 1635.0 cm^{-1} confirmed O-H and stretching vibrations of Ti-OH. This obtained hydroxyl band and Ti-OH are within the standard range [31].

3.2. XRD NiO Analysis. The synthesised nickel oxide was examined for the crystalline structure by utilising Cu-Kα radiation with wavelength (λ) = 1.5 Å. At the same time, the diffraction pattern was investigated by varying the angle of diffraction from 4.0° to 89.0°.

The XRD patterns are shown in Figure 4 for NiO at (111), (200), (202), (220), and (222) peak patterns reveal that NiO was successfully synthesised. Furthermore, the sharpness and high peak intensity prove that NiO has good crystallinity and phase purity. As seen in Figure 4, the sharp reflection peaks denote the presence of crystallite nickel oxide sizes. Also, the annealing temperature (400.0°C) adopted favoured the formation of crystalline structure in the synthesised nickel oxide nanoparticle formation. The JCPDS Card No. 47-1049 [32] was utilised to assess the d values of the XRD patterns. JCPDS Card indicates that NiO nanoparticles have a hexagonal structure. The average crystallite sizes D of nickel oxide nanoparticles were calculated, employing the Debye-Scherer equation shown in equation (3) [33] and full-width at half-maximum:

$$D = \frac{k\lambda}{\beta \cos\theta}, \quad (3)$$

where D is the crystallite size, k is the Scherer constant of the order of 0.9 associated with crystallite shape, and λ is the X-ray beam's wavelength in nanometers. These are tabulated in Table 2.

NiO nanoparticles have a crystallite size of 15.6 nm. This compares favourably with 21.0 nm obtained from a heat treatment [34] compared to 37.0 nm obtained from raffinate solution [35].

$$\delta = \frac{1}{D^2}. \quad (4)$$

The dislocation density of a crystalline material is the number of dislocations in unit volume. From equation (4), the dislocation density, δ, obtained was 0.0041. NiO nanoparticles were submitted to X-ray diffraction to determine purity phase and crystallinity. The XRD and morphology

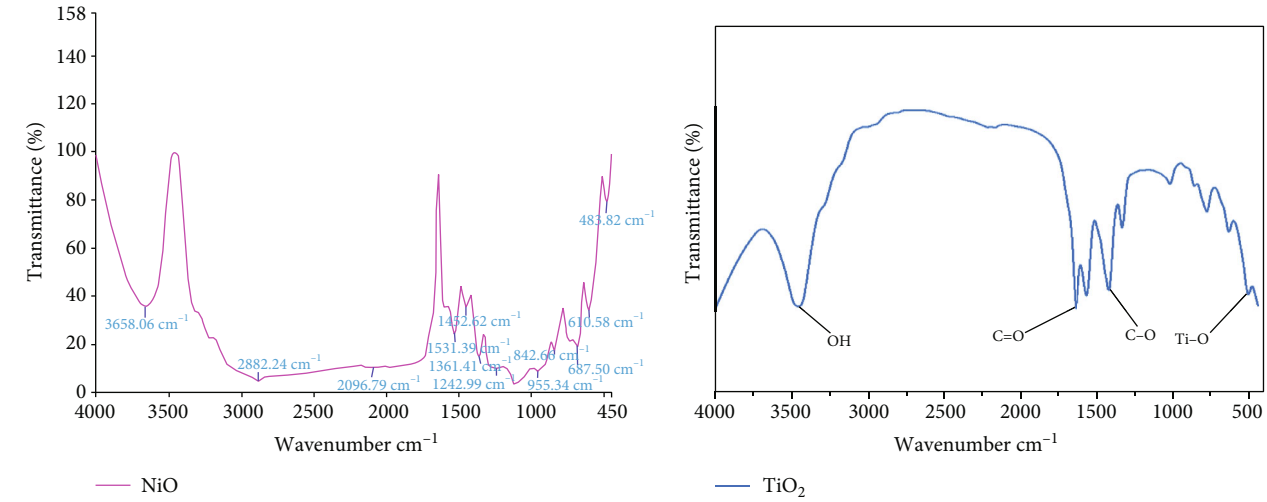

Figure 3: FTIR spectrum. (a) NiO. (b) TiO_2.

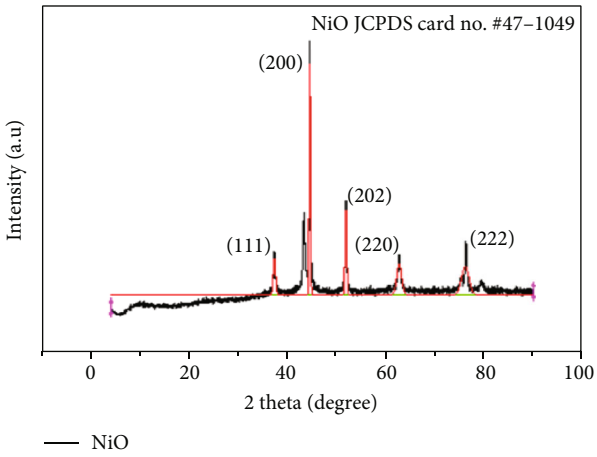

Figure 4: XRD pattern of nickel oxide nanoparticle.

Table 2: Structural parameters of the nanostructured NiO particles.

(hkl)	FWHM (°)	2θ (°)	θ (°)	D (nm)	d (Å)	δ (nm^{-2})
111.0	0.55	37.33	18.67	15.16	1.54	0.0044
200.0	0.32	44.55	22.28	27.28	1.54	0.0013
202.0	0.41	51.91	25.95	21.47	1.54	0.0022
220.0	1.14	62.96	31.48	8.18	1.54	0.014
222.0	1.74	76.28	38.14	5.79	1.54	0.03
				Avg $D = 15.6$		

(TEM, SEM) results corroborate this assertion. Hence, it was revealed that the produced NPs have exceptional crystalline properties.

3.3. XRD TiO_2 Analysis. The characterisation of titanium dioxide was examined for the crystalline structure by utilising Cu-Kα radiation of 1.54 Å wavelength, and equation (3) was used to calculate the crystalline size (D). The X-ray diffraction patterns of TiO_2 are shown in Figure 5. The primary peaks are visible in XRD patterns of (101) 25.3, (112) 37.8, (200) 48.1, (211) 55.1, (204) 62.7, and (215) 75.1 belong to the anatase phase of titanium dioxide. TiO_2 average crystalline size was found to be 41.2 nm using the Debye-Scherrer's equation. Table 3 gives detailed structural parameters of the TiO_2.

3.4. TEM NiO/TiO_2 Analysis. The TEM image of NiO showed the synthesised nickel oxides were joined closely to form nanospheres. The image showed the nanoparticles had uniform size, shape, and crystallinity. As determined using ImageJ, the average length of the nickel oxide nanoparticles was 18.7 nm. The nickel oxide nanoparticles existed as nanosheets with ultrathin nanostructure. The TiO_2 existed as agglomerated nanosheet. The TEM images confirmed the synthesis of pure nickel oxide, titanium dioxide nanosheets, as shown in Figure 6.

3.5. Particle Size. The average particle size of NiO is obtained as 18.7 nm and is plotted as shown in Figure 7(a). This value is in close range with the value of 20.0 nm obtained by Sone, Fuku [34]. Also, a histogram plot of the particle size analysis of TiO_2 obtained is shown in Figure 7(b). The average particle size for the TiO_2 was obtained to be 136.0 nm. This is within the range of 50.0 to 250.0 nm for TiO_2 particle sizes [36].

3.6. Morphology (SEM). Figure 8 gives the scanning electron microscope of the NiO and TiO_2 synthesised and subsequently deposited. The NiO is well arranged with a uniform, pinhole-free shape. A well-organised nanoseed of NiO structure is generated by using NaOH as a reducing agent to decrease the nickel acetate precursor. Hence, Figure 8(a) shows the high resolution of the SEM image of NiO NPs coated on the glass at 400.0°C annealing and Figure 8(b)

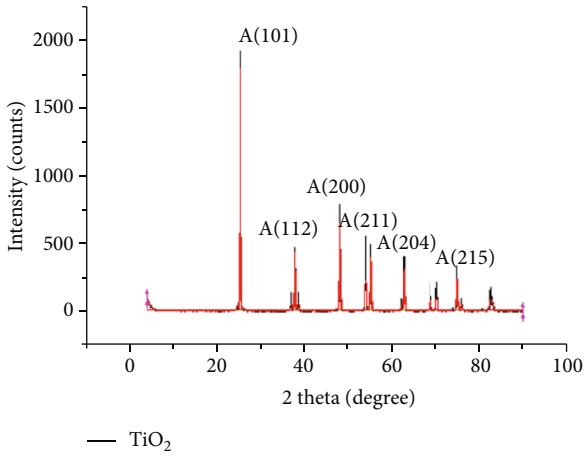

Figure 5: XRD pattern of titanium dioxide nanoparticle.

Table 3: Structural parameters of the nanostructured TiO2 particles.

(hkl)	FWHM (°)	2θ (°)	θ (°)	D (nm)	d (Å)	δ (nm^{-2})
101	0.15	25.30	12.65	56.59	1.54	0.000312
112	0.19	37.81	18.90	46.08	1.54	0.000471
200	0.22	48.05	24.03	40.99	1.54	0.000595
211	0.26	55.09	27.54	35.63	1.54	0.000788
204	0.28	62.72	31.36	34.67	1.54	0.000832
215	0.32	75.09	37.55	33.07	1.54	0.000914
				Avg $D = 41.17$		

for the TiO_2. The pure NiO and TiO_2 nanoparticles were clumped together within a diameter range, varying from 200.0 nm to 500.0 nm. Thus, NPS element composition was also approved or validated by energy-dispersive X-ray spectroscopy (EDX), whereby the maximum percentage of nickel and oxygen is 29.8 and 39.5 weight (%), respectively.

3.7. Elemental Composition of the Solar Thin Films (EDX). The elemental composition of each of the synthesised layers is shown in Figure 9. The major elements of NiO and TiO_2 were confirmed to be present from the EDX.

A study of NiO nanoparticles shows NaOH is a strong base that holds a direct source to decrease metal precursors, which is a view shared by numerous experts. A well nanoseed NiO structure is generated by using NaOH as a reducing agent to decrease the nickel acetate precursor. As a result, pure NiO nanoparticles possessed 29.8% Ni and 39.5% O, according to the proportions indicated in spectrum 5 of Figure 9(a). Conversely, the Si and C peaks of 0.9 and 29.9% weight were obtained, respectively, showing the silicon substrate and carbon-coated on the substrate material. According to Figure 10(b), it was reported that pure TiO_2 NPs had 28.9% Ti and 38.6% O while TiO_2 NPs had 16.1%, 3.3%, 10.3%, and 2.8% of Si, Ca, C, and Na, respectively. This demonstrated the presence and modification of PEI on TiO_2 nanoparticles (NPs).

4. The Solar Device Characterisation

The synthesised TiO_2 was spray deposited on the ITO-coated glass at 350.0°C as described by Ukoba, Eloka-Eboka [9] and was annealed. Thereafter, the NiO was deposited onto it using spin coating. They were stirred for an hour at approximately 60.0°C and spin coated. The films were annealed to approximately 400.0°C for about five minutes, and the process was repeated for five layers. The metal contact was gold and was deposited using the DC magnetron sputtering technique. This was characterised and here discussed. Figure 10 shows the photograph of the fabricated device.

4.1. Morphology of the Solar Device. The fabricated device was characterised using a scanning electron microscope, as shown in Figure 11. The layers are well aligned without pinholes and uniformly distributed on the surface of the ITO substrate. The thickness of NiO was obtained to be 200.0 nm using the stylus profilometer. The square-shaped solar device's dimensions are 25.0 mm by 25.0 mm, and the thickness was measured as 0.05 mm.

4.2. Elemental Composition of the Solar Device. Figure 12 shows the elements present in the p-NiO/n-TiO_2 device. It shows that Ti, O, and Ni are found in the fabricated device. Also, indium (In) was found in the EDX, which represents the ITO substrate used. Hence, NiO/TiO_2 is present in the solar cell device.

4.3. I-V Characterization. Figure 13 gives the I-V characteristic of the fabricated NiO/TiO_2 under light illumination and dark. The forward current experienced an increment as the voltage increased at room temperature under dark. The fabricated device had rectification properties due to the similarity between dark J-V plots and Shockley diode. The model CHEMAT TECHNOLOGY spin-coater KW-4A shown in Figure 1 was used for the deposition technique.

The characteristic (J-V) of the cell under illumination (100.0 mW/cm^2) obtained from the Keithley instrument is shown in Figure 13.

Table 4 gives values obtained from the J-V curve of the NiO/TiO_2 device. A value of 1.7 mA for J_{sc}, 370.0 mV for V_{oc}, and 0.38 for FF. The efficiency (η) was achieved at 3.7%.

4.4. Junction Parameters. From Figure 13, the value of n was obtained by the linearisation of equation (5) (by taking its logarithm) and taking its slope (which is directly related to n). The emissivity factor (ideality factor) was calculated from the dark illumination curve to be 1.09, and the barrier height was obtained to be 0.63 eV as obtained from equations (5) to (6).

The parameters were obtained using the thermionic emission model shown in equation (4) [37].

$$\mathrm{I} = I_0 \exp\left(\frac{qV}{nkT}\right), \tag{5}$$

where k is Boltzmann constant, saturation current is I_O, T is absolute temperature, the applied voltage is V, ideality factor is n, and electronic charge is q.

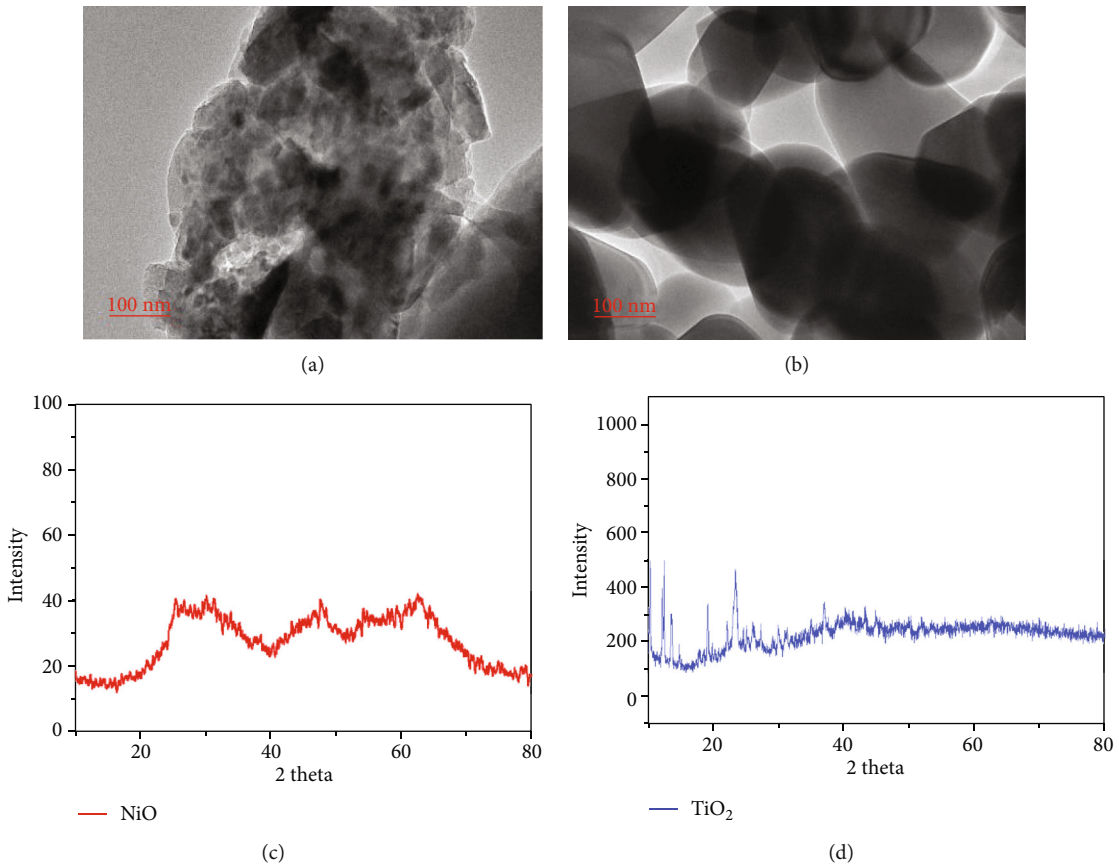

Figure 6: (a) TEM image of NiO. (b) TEM image of TiO_2. (c) Transmision spectrum of NiO. (d) Transmision spectrum of TiO_2.

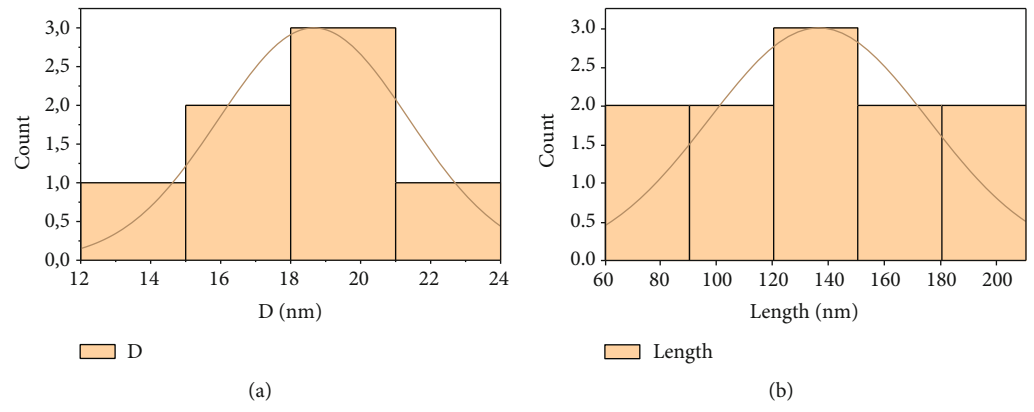

Figure 7: Particle size distribution of (a) NiO and (b) TiO_2.

The barrier height is obtained to be 0.63 eV using the reverse saturation current shown in equation (5) [38].

$$I_O = AA^* T^2 \exp\left(\frac{-q\varnothing_b}{kT}\right), \tag{6}$$

where barrier height is $\varnothing_b$, diode contact is A, and Richardson constant is A^*.

Using the Cheung and Cheung method [39], the series resistance was obtained to be $4.0 \times 10^4\ \Omega$ using equation (7).

$$I = I_O \exp\left[\frac{q(V - IR_s)}{nkT}\right]. \tag{7}$$

Also, equation (8) was used to determine the series resistance using the Nordes method [40], and it was found to be $2.7 \times 10^4\ \Omega$.

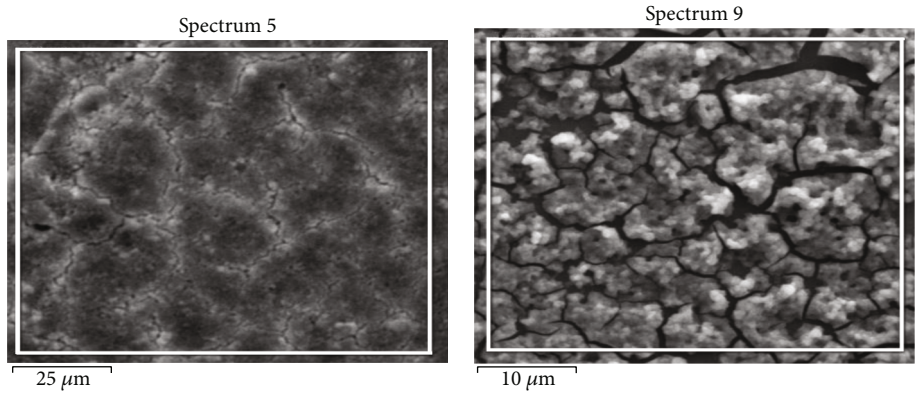

Figure 8: Scanning electron microscope of (a) NiO and (b) TiO_2.

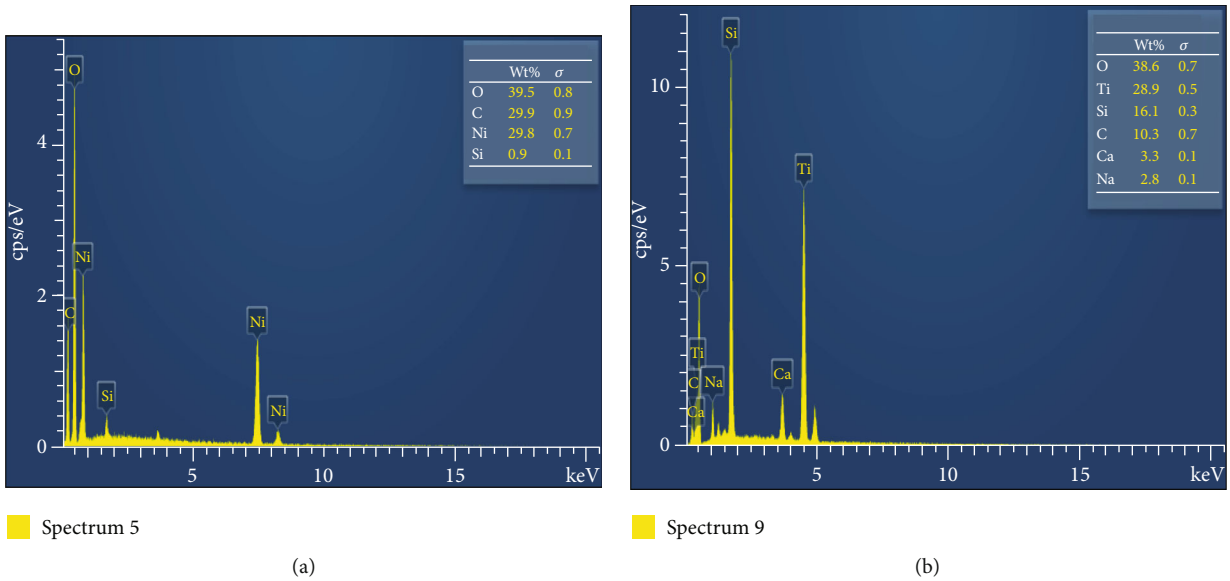

Figure 9: Elemental composition of (a) NiO and (b) TiO_2.

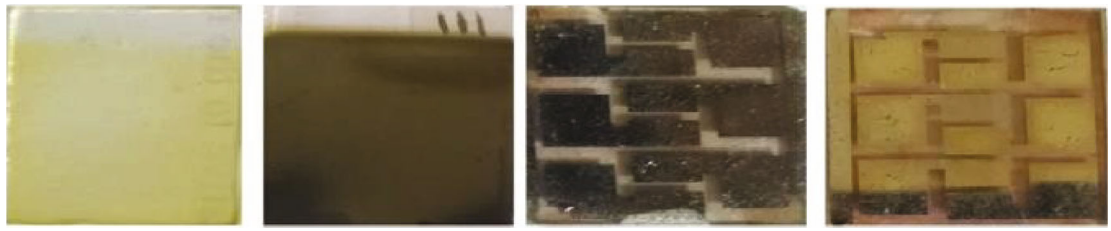

Figure 10: Photograph of the fabricated device.

$$R_s = \frac{kT(\gamma - n)}{qI}, \tag{8}$$

where γ is the integer (dimensionless) greater than n.

It is worth knowing that Norde's method is used for full voltage range forward bias, and Cheung's method is used for high voltage region. The obtained ideality factor is greater than the 1.02 standard value [41]. This may be attributed to interface properties existing between TiO_2 and NiO. Although, the effect of hole depletion and accelerated recombination of the electron may also account for this difference [42].

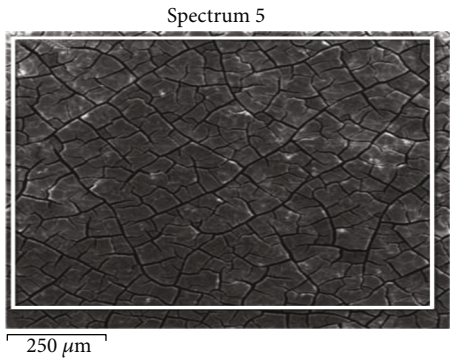

Figure 11: Morphology of the solar device.

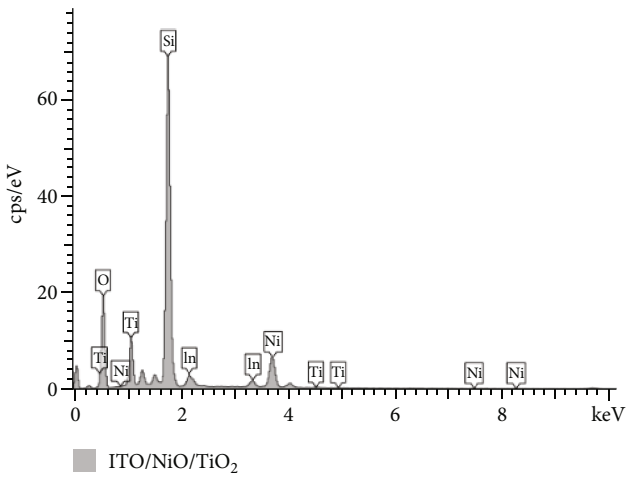

Figure 12: The p-NiO/n-TiO_2 solar cell device EDX.

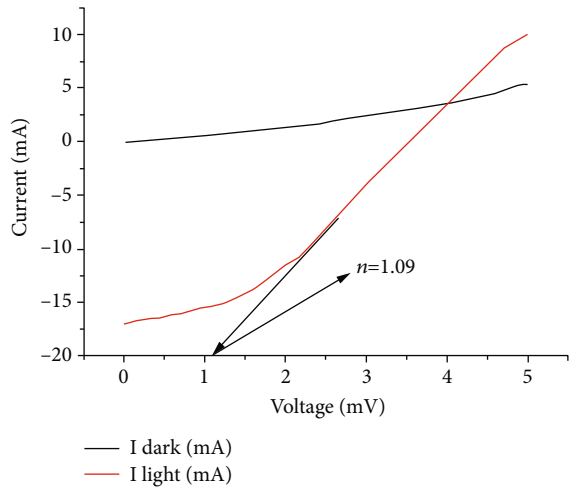

Figure 13: NiO/TiO_2 heterojunction solar cells I-V curve under illumination and in the dark.

The limitations of semiconductor diode include high noise level at high frequency and presence of reverse saturation current.

Table 4: The fabricated NiO/TiO_2 solar cell parameters.

Device	V_{oc} (mV)	V_{max} (mV)	J_{sc} (mA)	J_{max} (mA)	FF (%)	η (%)
NiO/ TiO_2	370.0	174	1.70	13.0	*38.0*	*3.7*

5. Conclusion

This study shows the fabrication of NiO/TiO_2 solar cells for photovoltaic application. The NiO and TiO_2 were synthesised and deposited. The deposited films were characterised before the final device fabrication of the solar cells. The NiO nanoparticles had a crystallite size of 15.6 nm and particle size of 18.7 nm, while TiO_2 had a crystalline size of 41.2 nm and a particle size of 136.0 nm. The dislocation density, δ, was obtained to be 0.0041. An efficiency of 3.7% and a filling factor of 38.0% under illumination (100.0 mW/cm^2) was recorded. This represents an improvement in the existing efficiency recorded for the metal oxide. It also shows promise that NiO can be used for efficient deposition of highly efficient solar cells. The short circuit obtained is in tandem with the bandgap of the materials used. The ideality factor was obtained to be 1.09, and the barrier height was obtained as 0.63.

Appendix

Spin coater equipment used for the fabrication p-NiO/n-TiO2.

The model CHEMAT TECHNOLOGY spin-coater KW-4A was used for the deposition technique.

The crucial parameters used were as follows:
Times (30 sec).
Standard rotation speed (1000 rpm).
Speeds
Front panel controls:
Digital readout in speed 1,000 rpm
Timer controls, stage I and stage II
Speed controls, stage I and stage II
Control switch
Vacuum switch
Power switch
Start switch
Specifications:
Stage 1: 500-2,500 rpm, 2-18 seconds 2-stage spinning
Stage 2: 1,000-8,000 rpm, 3-60 seconds
Power: 115 VAC, 60 Hz, 1 Amp 220 VAC, 50 Hz, 1 Amp
Vacuum: 2.1 CFM

Data Availability

The data in this paper can be made available upon request.

Conflicts of Interest

The authors declare that there is no conflict of interest arising from this research.

Acknowledgments

The authors appreciate funding from National Research Foundation (NRF) of South Africa and URC of the University of Johannesburg.

Supplementary Materials

Supplementary 1. The graphical abstract summarises the entire manuscript graphically by using shapes.

Supplementary 2. Highlights document gives the key points of the manuscript. It gives the major highlights contained in the manuscript.

References

[1] K. O. Ukoba, A. C. Eloka-Eboka, and F. L. Inambao, *Review of solar energy inclusion in Africa: a case study of Nigeria*, p. 12, 2017.

[2] H. Park, D. Kim, J. Jung et al., "HF etched glass substrates for improved thin-film solar cells," *Heliyon*, vol. 4, no. 10, article e00835, 2018.

[3] Y. Qin, J. Song, Q. Qiu et al., "High-quality NiO thin film by low-temperature spray combustion method for perovskite solar cells," *Journal of Alloys and Compounds*, vol. 810, article 151970, 2019.

[4] M. Khan, K. Bhatti, R. Qindeel, N. Alonizan, and H. S. Althobaiti, "Characterizations of multilayer ZnO thin films deposited by sol-gel spin coating technique," *Results in physics*, vol. 7, pp. 651–655, 2017.

[5] S. Handani, Emriadi, D. Dahlan, and S. Arief, "Enhanced structural, optical and morphological properties of ZnO thin film using green chemical approach," *Vacuum*, vol. 179, article 109513, 2020.

[6] H. Zaka, B. Parditka, Z. Erdélyi, H. Atyia, P. Sharma, and S. Fouad, "Investigation of dispersion parameters, dielectric properties and opto- electrical parameters of ZnO thin film grown by ALD," *Optik*, vol. 203, article 163933, 2020.

[7] T. Ouslimane, L. Et-Taya, L. Elmaimouni, and A. Benami, "Impact of absorber layer thickness, defect density, and operating temperature on the performance of $MAPbI_3$ solar cells based on ZnO electron transporting material," *Heliyon*, vol. 7, no. 3, article e06379, 2021.

[8] M. Y. Ali, M. Khan, A. T. Karim, M. M. Rahman, and M. Kamruzzaman, "Effect of Ni doping on structure, morphology and opto-transport properties of spray pyrolised ZnO nano-fiber," *Heliyon*, vol. 6, no. 3, article e03588, 2020.

[9] K. Ukoba, A. Eloka-Eboka, and F. Inambao, "Review of nanostructured NiO thin film deposition using the spray pyrolysis technique," *Renewable and Sustainable Energy Reviews*, vol. 82, pp. 2900–2915, 2018.

[10] H.-Y. Liu, C.-C. Hung, and W.-C. Hsu, "Deposition of oxide thin films by ultrasonic spray pyrolysis deposition for InGaZnO thin-film transistor applications," *IEEE Electron Device Letters*, vol. 39, pp. 1–3, 2018.

[11] G. Korotcenkov and B. Cho, "Spray pyrolysis deposition of undoped SnO_2 and In_2O_3 films and their structural properties," *Progress in Crystal Growth and Characterization of Materials*, vol. 63, no. 1, pp. 1–47, 2017.

[12] M. Khan, K. Bhatti, R. Qindeel, H. S. Althobaiti, and N. Alonizan, "Structural, electrical and optical properties of multilayer TiO_2 thin films deposited by sol-gel spin coating," *Results in physics*, vol. 7, pp. 1437–1439, 2017.

[13] R. Barir, B. Benhaoua, S. Benhamida, A. Rahal, T. Sahraoui, and R. Gheriani, "Effect of precursor concentration on structural optical and electrical properties of NiO thin films prepared by spray pyrolysis," *Journal of Nanomaterials*, vol. 2017, Article ID 5204639, 10 pages, 2017.

[14] A. Adeoye, E. Ajenifuja, S. Alayande, E. Ogunmola, O. Adeyemi, and A. Fasasi, "Effects of Zn doping concentration on the optical and photovoltaic properties of $Zn_xPb_{1-x}S$ thin film-based solar cell prepared by chemical spray pyrolysis," *SN Applied Sciences*, vol. 2, no. 9, pp. 1–10, 2020.

[15] K. O. Ukoba, F. L. Inambao, and A. C. Eloka-Eboka, "Fabrication of affordable and sustainable solar cells Using NiO/TiO2 P-N heterojunction," *International Journal of Photoenergy*, vol. 2018, Article ID 6062390, 7 pages, 2018.

[16] H.-S. Kim, J. E. Park, M. Patel et al., "Optically transparent and electrically conductive NiO window layer for Si solar cells," *Materials Letters*, vol. 174, pp. 10–13, 2016.

[17] H. Lee, Y.-T. Huang, M. W. Horn, and S.-P. Feng, "Engineered optical and electrical performance of rf-sputtered undoped nickel oxide thin films for inverted perovskite solar cells," *Scientific Reports*, vol. 8, no. 1, pp. 1–10, 2018.

[18] G. Boschloo and A. Hagfeldt, "Spectroelectrochemistry of nanostructured NiO," *The Journal of Physical Chemistry B*, vol. 105, no. 15, pp. 3039–3044, 2001.

[19] G. T. Anand, R. Nithiyavathi, R. Ramesh, S. John Sundaram, and K. Kaviyarasu, "Structural and optical properties of nickel oxide nanoparticles: investigation of antimicrobial applications," *Surfaces and Interfaces*, vol. 18, article 100460, 2020.

[20] F. Taghizadeh, "The study of structural and magnetic properties of NiO nanoparticles," *Optics and Photonics Journal*, vol. 6, no. 8, pp. 164–169, 2016.

[21] M. Bonomo, D. Dini, and F. Decker, "Electrochemical and photoelectrochemical properties of nickel oxide (NiO) with nanostructured morphology for photoconversion applications," *Frontiers in chemistry*, vol. 6, p. 601, 2018.

[22] S. A. Rawool, M. R. Pai, A. M. Banerjee et al., "*pn* Heterojunctions in $NiO:TiO_2$ composites with type-II band alignment assisting sunlight driven photocatalytic H_2 generation," *Applied Catalysis B: Environmental*, vol. 221, pp. 443–458, 2018.

[23] J. H. Heo, S. H. Im, J. H. Noh et al., "Efficient inorganic-organic hybrid heterojunction solar cells containing perovskite compound and polymeric hole conductors," *Nature photonics*, vol. 7, no. 6, pp. 486–491, 2013.

[24] P. Qin, S. Tanaka, S. Ito et al., "Inorganic hole conductor-based lead halide perovskite solar cells with 12.4% conversion efficiency," *Nature communications*, vol. 5, no. 1, pp. 1–6, 2014.

[25] A. S. Subbiah, A. Halder, S. Ghosh, N. Mahuli, G. Hodes, and S. K. Sarkar, "Inorganic hole conducting layers for perovskite-based solar cells," *The journal of physical chemistry letters*, vol. 5, no. 10, pp. 1748–1753, 2014.

[26] K. O. Ukoba, A. C. Eloka-Eboka, and F. L. Inambao, "Experimental optimization of nanostructured nickel oxide deposited by spray pyrolysis for solar cells application," *International Journal of Applied Engineering Research*, vol. 13, no. 6, pp. 3165–3173, 2018.

[27] M. R. Das, A. Roy, S. Mpelane, A. Mukherjee, P. Mitra, and S. Das, "Influence of dipping cycle on SILAR synthesized NiO thin film for improved electrochemical performance," *Electrochimica Acta*, vol. 273, pp. 105–114, 2018.

[28] Z. Chen, T. Dedova, I. O. Acik, M. Danilson, and M. Krunks, "Nickel oxide films by chemical spray: effect of deposition temperature and solvent type on structural, optical, and surface properties," *Applied Surface Science*, vol. 548, article 149118, 2021.

[29] Y. Zhu, W. Chu, N. Wang et al., "Self-assembled Ni/NiO/RGO heterostructures for high-performance supercapacitors," *RSC advances*, vol. 5, no. 95, pp. 77958–77964, 2015.

[30] S. Mugundan, B. Rajamannan, G. Viruthagiri, N. Shanmugam, R. Gobi, and P. Praveen, "Synthesis and characterization of undoped and cobalt-doped TiO_2 nanoparticles via sol–gel technique," *Applied Nanoscience*, vol. 5, no. 4, pp. 449–456, 2015.

[31] A. León, P. Reuquen, C. Garín et al., "FTIR and Raman characterization of TiO2 nanoparticles coated with polyethylene glycol as carrier for 2-methoxyestradiol," *Applied Sciences*, vol. 7, no. 1, p. 49, 2017.

[32] A. Kumar and P. Sahay, "Lithium doping in spray-pyrolyzed NiO thin films: results on their microstructural, optical and electrochromic properties," *Applied Physics A*, vol. 127, no. 4, pp. 1–17, 2021.

[33] R. Jenkins and L. R. Snyder, *Introduction to X-Ray Powder Diffractometric*, John Wiley & Sons, New Jersey, 1996.

[34] B. Sone and M. Maaza, "Physical & electrochemical properties of green synthesized bunsenite NiO nanoparticles via Callistemon viminalis' extracts," *International Journal of Electrochemical Science*, vol. 11, pp. 8204–8220, 2016.

[35] B. Ebin, "Simple preparation of Ni and NiO nanoparticles using raffinate solution originated from spent NiMH battery recycling," *Journal of Inorganic and Organometallic Polymers and Materials*, vol. 28, no. 6, pp. 2554–2563, 2018.

[36] D. Li, H. Song, X. Meng et al., "Effects of particle size on the structure and photocatalytic performance by alkali-treated TiO_2," *Nanomaterials*, vol. 10, no. 3, p. 546, 2020.

[37] J. M. Shah, Y.-L. Li, T. Gessmann, and E. F. Schubert, "Experimental analysis and theoretical model for anomalously high ideality factors (n≫2.0) in AlGaN/GaNp-njunction diodes," *Journal of applied physics*, vol. 94, no. 4, pp. 2627–2630, 2003.

[38] Ş. Karataş and A. Türüt, "Electrical properties of Sn/p-Si (MS) Schottky barrier diodes to be exposed to ^{60}Co _γ_ -ray source," *Nuclear Instruments and Methods in Physics Research Section A: Accelerators, Spectrometers, Detectors and Associated Equipment*, vol. 566, no. 2, pp. 584–589, 2006.

[39] S. Cheung and N. Cheung, "Extraction of Schottky diode parameters from forward current-voltage characteristics," *Applied physics letters*, vol. 49, no. 2, pp. 85–87, 1986.

[40] H. Norde, "A modified forward I-V plot for Schottky diodes with high series resistance," *Journal of Applied Physics*, vol. 50, no. 7, pp. 5052-5053, 1979.

[41] R. Gupta and R. Singh, "Electrical properties of junction between aluminium and poly(aniline)-poly(vinyl chloride) composite," *Materials chemistry and physics*, vol. 86, no. 2-3, pp. 279–283, 2004.

[42] R. Singh and A. K. Narula, "Junction properties of aluminum/polypyrrole (polypyrrole derivatives) Schottky diodes," *Applied physics letters*, vol. 71, no. 19, pp. 2845–2847, 1997.